Material Comparison of an Automotive Rear Spoiler using FEA

Roshan Ladha

Received September 10, 2025
Accepted October 24, 2025
Electronic access October 28, 2025

Rear spoilers must balance aerodynamic efficiency with structural resilience. This study evaluates a fixed-geometry spoiler manufactured from ABS, aluminum 6061-T6, and quasi-isotropic CFRP using finite-element analysis under three representative pres- sure loads (520, 1 040, and 1 560 Pa) derived from dynamic pressure estimates. Alu- minum demonstrated the smallest tip deflections (0.0540.162 mm) with consistently high safety margins (SF 7.3 at 1 560 Pa). CFRP provided similarly low deflections (0.1650.495 mm), with adequate safety (SF 4.85). When normalized by mass, alu- minum exhibited the best static stiffness-to-mass (smallest $\frac{\Delta}{\rho}$), while CFRP achieved the best dynamic stiffness-to-mass (largest $\frac{f_1}{\rho}$). By contrast, ABS exhibited substan- tial deformation (1.825.45 mm) and dropped below unity safety at the highest loading condition (SF 0.96), indicating failure onset. The first-mode natural frequencies were approximately 25.7 Hz for aluminum, 21.6 Hz for CFRP, and 7.26 Hz for ABS, with the ABS mode falling far short of the 30 Hz vibration-resistance target and thus disqualifying it as a viable material choice for this geometry. Overall, the results indicate aluminum is preferred when minimizing deflection or maximizing static stiffness-per-mass, CFRP is advantageous where mass reduction and dynamic stiffness-per-mass are prioritized, and ABS is unsuitable for structurally loaded spoilers.

Introduction

Automotive rear spoilers generate down-force that enhances vehicle stability at high speeds. In high performance vehicles, rear spoilers improve track performance and vehicle control. As the automotive industry improves efficiency, moving towards more lightweight designs, the use of advanced composites in spoilers becomes necessary. While previous studies have emphasized aerodynamic design assessment of spoiler profiles, relatively fewer have evaluated how structural materials affect performance metrics. This is especially the case with the invention of advanced composites. Testing advanced composites is crucial to understand how these materials can be used for improvements in the automotive industry. For fixed geometry, the stiffness-to-weight characteristics of the material dictate deformation, stress distribution, and fatigue life.

Background

Foundational studies on road-vehicle aerodynamics and spoiler effects provide the context for this work, including canonical wake investigations and spoiler aeroelasticity analyses[1,2]. For spoilers with fixed geometry, material selection becomes the primary driver of mechanical behavior. The choice of material influences both structural stiffness and deflection. As automotive manufacturers strive to reduce vehicle weight without compromising performance or safety, understanding how different materials respond to aerodynamic forces becomes essential. Finite Element Analysis (FEA) offers a noninvasive approach to evaluate and isolate the mechanical response of materials, making it the ideal methodology for this comparative research study.

This work therefore addresses the following research question: How does material choice influence deflection, stress, and safety factor for a fixed spoiler geometry under realistic aerodynamic loading? We evaluate three materials widely used in automotive body-exterior applicationsABS, Aluminum 6061-T6, and quasi-isotropic CFRP[3,4]. To answer this research question, we begin from an open-source geometry of a spoiler that allows us to perform a structural analysis. This study establishes baseline performance for the spoiler using various materials under loading conditions.

Methods

Spoiler Geometry

The analysis uses an open-source CAD assembly from the GrabCAD library. The spoiler consists of four main components: the main wing, endplates, brackets, and mounting bases. The main wing is a constant-chord, flat-plate element modeled as a solid body without internal spars. Its bending stiffness is derived entirely from the full-depth section of the wing. The endplates are two thin plates bolted to the wing using a pair of generic fasteners. In the finite element model, these fasteners are idealized as bonded contacts applied across the bolt footprints to simplify the simulation. The brackets are dual sheet-metal structures

© The National High School Journal of Science 2025

featuring three concentric lightening holes for weight reduction. These brackets, or pedestals, are slightly raked forward to ensure aerodynamic clearance and are connected to the underside of the wing using clevis-style pins, which are represented in the model as frictionless cylindrical joints. Finally, the mounting bases are rectangular base plates located at the foot of each pedestal. These bases are rigidly secured to the vehicle deck and defined as fixed supports in the simulation. The spoiler geometry obtained from GrabCAD was validated against established automotive spoiler design parameters documented in literature to ensure aerodynamic realism and representativeness of production vehicle configurations. Dimensional analysis confirmed that the models key geometric parameters fall within the typical range of passenger vehicle spoilers. These specifications align with established airfoil profiles commonly employed in automotive spoiler design. Comparative analysis with documented real-world spoiler dimensions from academic CFD studies shows that the GrabCAD model exhibits geometric characteristics consistent with production automotive spoilers used in vehicles. While absolute aerodynamic optimization was not the primary objective of this material comparison study, the geometric validation ensures that the model represents realistic loading conditions and structural dimensions typical of automotive spoiler applications, thereby providing a meaningful basis for comparative material analysis without compromising the validity of the mechanical property comparisons[5–7].

Material Models

Material choice has a profound impact on a spoilers static strength, stiffness, weight, and dynamic, or modal, behavior. This study compares three common materials ABS (Acrylonitrile Butadiene Styrene) plastic, aluminum 6061-T6, and carbon-fiber-reinforced polymer (CFRP) to illustrate how their differing properties influence structural performance. The selection of ABS, aluminum 6061-T6, and quasi-isotropic carbon fiber reinforced polymer represents three distinct material categories that span the automotive spoiler market from mass production to high-performance applications, each offering unique advantages in cost, manufacturing, and performance characteristics. ABS plastic serves as the cost-effective baseline material, widely utilized in automotive exterior components due to its excellent moldability, impact resistance, and manufacturing economy, with studies demonstrating comparable mechanical properties to natural fiber alternatives in spoiler applications.

Aluminum 6061-T6 represents the premium metallic option, offering superior machinability and strength-to-weight ratio characteristics essential for high-performance automotive applications. Academic research on 6061-T6 aluminum machining demonstrates its excellent surface finish capabilities and mechanical properties that make it suitable for precision automotive components. Quasi-isotropic CFRP represents the highest performance tier, offering exceptional strength-to-weight ratios but at significantly higher material costs, making it primarily suitable for luxury and motorsport applications. Current research indicates that while CFRP materials can achieve superior mechanical properties, their adoption remains limited by manufacturing costs and processing complexity, though advancing manufacturing techniques continue to improve their commercial viability for high-performance automotive exterior components[8–11]. Table 1 summarizes key properties of each material and elastic constants to be used. Below, we pro- vide context on each materials characteristics, advantages, and drawbacks, and how these relate to spoiler performance. Accurate representation of material behavior is essential in finite-element simulations to predict stress distribution and deformation under aerodynamic loading. Therefore, materials were modeled according to their mechanical nature: ABS and aluminum as isotropic, and CFRP as quasi-isotropic due to its layered composite structure. This means that CFRPs directional stiffness assumed uniform in-plane properties by orienting plies in multiple directions.

Table 1 Column Definitions

The parameters listed in Table 1 define the mechanical behavior of each material used in the analysis. Below, each parameter is defined:

- ρ (density). Mass per unit volume presented in gcm^{-3}; it directly influences the inertial terms and overall weight of the spoiler assembly.
- E or $E_1/E_2/E_3$ (Youngs modulus). Resistance to uniaxial deformation. For isotropic ABS and aluminum, a single modulus E suffices; for orthotropic CFRP, three principal moduli (E_1, E_2, E_3) capture directional stiffness
- G (shear modulus). Material rigidity under shear loading; for composites, an in-plane equivalent value is specified.
- ν (Poissons ratio). Lateral contraction ratio in uniaxial tension, required for con- stitutive matrix completion.
- $\frac{\sigma^T}{\sigma^C}$ (tensile/compressive strength). Ultimate strengths used to gauge failure indices.
- τ(shear strength). Maximum in-plane shear strength used for shear-governed safety checks. For isotropic materials (ABS, aluminum) this is the ultimate shear strength from datasheets; for CFRP it corresponds to the in-plane lamina shear allowable.

Strengths and safetyfactor convention

For Aluminum 6061T6, Table 1 lists the ultimate tensile strength, but all aluminum safety factors in Sec. 3.1 are computed against the yield strength to avoid permanent set. For ABS, the governing limit under bending is the tensile/flexural allowable; we use a conservative tensile value for SF calculations. For the

© The National High School Journal of Science 2025

Table 1 Material properties including density, Youngs modulus, shear modulus, Poissons ratio, tensile strength, and shear strength [12–16].

Material	ρ (g/cm^3)	E or $E_1/E_2/E_3$ (GPa)	G (GPa)	ν	σ_T / σ_C (MPa)	τ (MPa)
ABS	1.03	2.2	0.8	0.39	40	34
Aluminum 6061-T6	2.70	69	26	0.33	310	207
CFRP (quasi-iso)	1.60	290	5	0.30	400	70

quasi- isotropic CFRP, we report SF with respect to the in-plane fiber-direction tensile/compressive allowable.

Normalization convention

Because the spoiler geometry and volume are identical across materials, mass is proportional to density ($m = \rho V$). To compare stiffness-to-mass performance, results are therefore normalized by density and reported as displacement per density ($\frac{\Delta}{\rho}$) and first-mode frequency per density ($\frac{f_1}{\rho}$).

Aerodynamic Loading Scenarios

A calculated value of $p \approx 1040Pa$ is applied uniformly over the spoilers planform area to represent aerodynamic loading. Three scalar cases are considered, as shown in Table 2. These loading scenarios are intended to approximate the range of downforce levels a high- performance spoiler may encounter under realistic driving conditions, such as high-speed cornering or straight-line acceleration. This enables a comparative evaluation of structural performance under varying aerodynamic demands. These pressures therefore represent highway to high-performance conditions. The uniform pressure assumption is a conservative simplification; the true surface loading is non-uniform and depends on geometry and flow state.

The aerodynamic pressure loads (520, 1 040, and 1 560 Pa) were derived using the dynamic pressure equation:

$$p = \frac{1}{2}\rho V^2 \tag{1}$$

where p is dynamic pressure, $\rho = 1.225 kg/m^3$ (standard air density), and V is vehicle speed. Simulations considered three representative speeds: 80 km/h (22.22 m/s), 120 km/h (33.33 m/s), and 160 km/h (44.44 m/s). Substituting:

$$p_{80} = 1 \times 1.225 \times (22.22)^2 \approx 302 \text{ Pa}$$
$$p_{120} = 1 \times 1.225 \times (33.33)^2 \approx 680 \text{ Pa}$$
$$p_{160} = 1 \times 1.225 \times (44.44)^2 \approx 1{,}207 \text{ Pa}.$$

These values were then scaled upward to account for spoiler planform effects, flow separation, and empirical amplification observed in published studies of rear spoilers resulting in the applied loads of 520, 1 040, and 1 560 Pa used in these simulations [17–19].

Table 2 Pressure loading scenarios applied to the spoiler surface in ANSYS finite-element simulations, representing increasing severity levels.

Case	Pressure (Pa)	Design Scenario
LC1	520	Service (50%)
LC2	1,040	Design (100%)
LC3	1,560	Ultimate (150%)

Finite Element Procedure

The finite-element method (FEM) converted the spoilers elasticity problem into the discrete system

$$Ku = F$$

The solid was meshed into elements with nodal degrees of freedom; polynomial shape functions and the virtual-work statement produced element stiffness matrices, which were assembled into the global system. Solving yielded nodal displacements, and strains and stresses were then recovered from standard straindisplacement and constitutive relations.

Mesh Description

The spoiler assembly was discretized using a 3D mesh composed of elements, well-suited for capturing curvature and geometric complexity. Mesh refinement was applied at stress-critical locations, including the bracket holes, clevis joints, and wing-to-bracket interfaces. The final mesh contained approximately 29,000 elements and 58,000 nodes. Figures of the spoiler mesh are provided below from three different angles.

To justify the working mesh of 29,000 elements, we performed an hrefinement check using three meshes (coarse 15k, medium 29k, fine 60k). Boundary conditions and loads were identical across meshes, with local refinement around fillets and mounting features. The governing response quantities were (i) maximum tip displacement and (ii) peak von Mises stress at the hotspot. Between the medium and fine meshes, the change in tip displacement was below a 2% tolerance and the change in peak stress was within a 5% tolerance, while the location of the stress hotspot remained unchanged. Accordingly, the 29k-element mesh was selected as the coarsest mesh that satisfies these convergence criteria, providing mesh- independent results. For modal analysis, the first natural frequency varied negligibly between the medium and fine meshes (within 2%), supporting the

same mesh choice.
The finite element mesh was composed of tetrahedral elements to capture complex spoiler geometry. Tetrahedral elements are the industry standard for intricate solid bodies and provide an effective balance of geometric fidelity and computational efficiency for the curved surfaces of the spoiler[20].

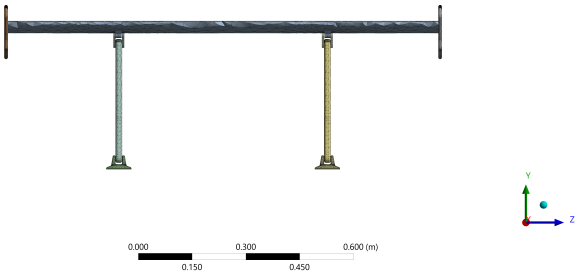

Fig. 1 Finite element mesh of the spoiler assembly front view.

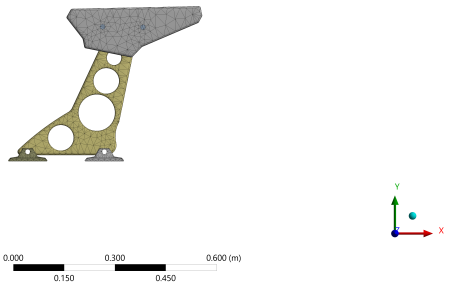

Fig. 2 Finite element mesh of the spoiler assembly side view.

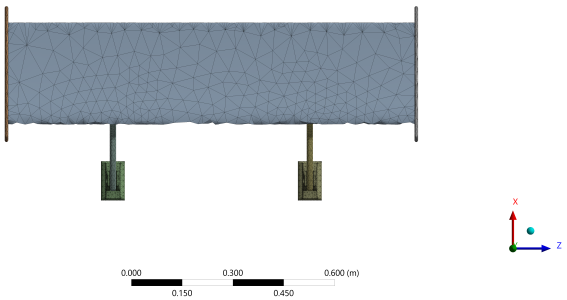

Fig. 3 Finite element mesh of the spoiler assembly top view.

Boundary Conditions

To replicate an in-service spoiler mounting scenario, the spoiler assembly is constrained by two fixed supports assigned to the underside of the pedestal base plates, treated as rigidly bolted to the vehicle deck. Real deck-lid/body panels have finite compliance; this study idealizes the mounts as rigid and does not include that flexibility. The aerodynamic pressure load is introduced as a spatially uniform pressure acting normal to the upper (suction-side) surface of the wing. Load magnitudes correspond to the service, design, and ultimate cases summarized in Table 2.

Modal Analysis

Modal analysis determines the natural frequencies and corresponding mode shapes of a struc- ture in the absence of external damping. We compute undamped eigenfrequencies and mode shapes to compare materials on a consistent basis and to assess separation from a 30 Hz target. For light damping typical of metals, polymers, and CFRP laminates (order of a few percent of critical), the frequency shift is on the order of 103 relative (negligible for ranking and threshold checks). Damping chiefly governs response amplitudes near resonance rather than the eigenfrequencies themselves. Because we do not perform a forced-response analysis here, omitting damping avoids introducing uncertain estimates for joint, material, and interface losses without affecting the conclusions about mode placement or stiffness comparisons[21–25]. Each natural frequency represents a resonant condition at which the structure can oscillate with minimal input energy. Knowledge of these frequencies is critical because if operational or environmental excitation coincides with a natural frequency, dynamic amplification and potentially catastrophic fatigue can occur.
A modal analysis solver is used to compute the first six fundamental frequencies. Key outputs collected include natural frequencies and mode shapes with qualitative deformation patterns.
For a spoiler, the most concerning scenario is a low-frequency bending or torsional mode that coincides with road-induced vibration. Therefore, we aim to keep the first structural mode above 30 Hz for this vehicles spoiler.

Results and Discussion

Structural Analysis

The following tables show the effects of each of the prescribed loading cases on the spoiler for each material, solving for maximum tip displacement and peak stress. Across materials, load scaling is approximately linear in both displacement and stress, as expected for small-deflection elastic response, enabling direct comparison of safety-factor trends. To aid interpretation,

© The National High School Journal of Science 2025

concise observations are provided immediately after each table. For ABS, the aerodynamic loading on the spoiler induces global bending, placing the lower surface in tension and the upper surface in compression. While shear stresses are present near the supports, the critical stresses arise in the tensile region of the cross-section. Since ABS generally exhibits lower tensile strength compared to compressive strength, the safety factor was evaluated with respect to the tensile/flexural limit, which represents the governing failure mode [26,27].

For CFRP, the quasi-isotropic laminate exhibits anisotropic behavior, with comparatively high strength in fibr tension but reduced strength in compression and in-plane shear. Under bending, the laminate experiences significant compressive loading on the upper surface as well as interlaminar shear. Consequently, the compressive and shear limits were identified as the governing conditions for the safety factor, as these modes are more likely to control failure than the laminate tensile response [28–30].

Interpretation (Aluminum). Displacements remain submillimetric across all loads, indicating high stiffness. Safety factors are computed using σ_y (yield) rather than σ_u, consistent with avoiding permanent set. Peak stresses scale proportionally with pressure yet remain well below the stated strength, yielding safety factors ¿7 even at LC-3. This suggests adequate static margin with minimal deformation for the aluminum spoiler in the examined regime.

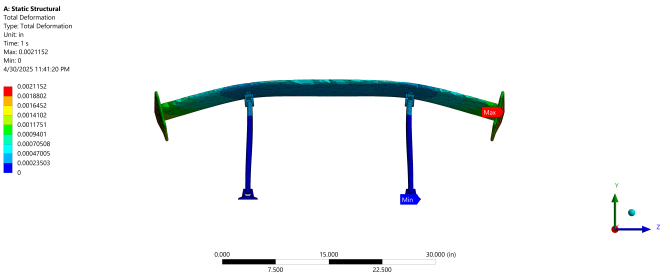

Fig. 4 Total deformation plot of the spoiler under Load Case LC-1 with Aluminum Alloy, shown with a 2 deformation scale factor. Deformation is exaggerated to illustrate bending and displacement characteristics.

Interpretation (ABS) table 4. Displacement is an order of magnitude larger than aluminum under identical loading, reflecting the lower stiffness. Safety factors for ABS are evaluated against the tensile/flexural limit. The safety factor trends downward with pressure and drops below unity at LC-3, indicating incipient failure under the highest aerodynamic load. Because bending places the lower face in tension, the tensile/flexural limit governs this assessment.

Interpretation (CFRP) table 5. Displacements are low despite the light weight, illustrating the favor- able stiffness-to-mass characteristics of the laminate. CFRP safety factors reported in Table 5 use the in-plane tensile/compressive allowable. Safety factors remain comfortably above unity across all load cases.

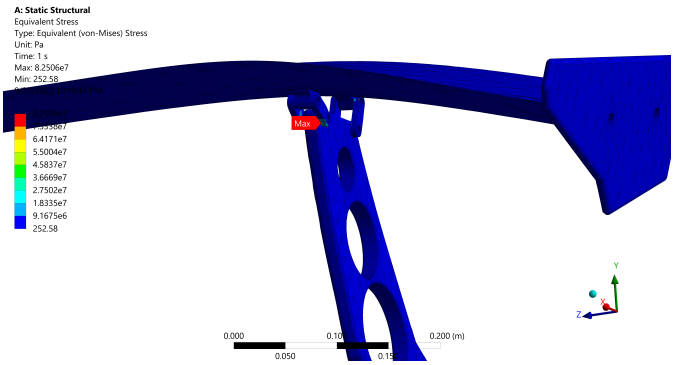

Fig. 5 Critical region at the connection point of the spoiler. The view highlights the mount holes and fillets where stress concentrations occur; this area was locally refined to capture steep gradients (e.g., smaller target element size at the clevis and wingbracket interface).

Consistent with laminate behavior, compressive and in-plane shear al- lowables govern the margin under bending rather than tensile strength.

Modal Analysis

The following tables show the first six fundamental frequencies of the spoiler for each material.

Interpretation (Modal) table 6,7,8. The ABS spoiler exhibits the lowest fundamental frequency, indicating greater susceptibility to low-frequency excitation and potential ride-induced resonance. Aluminum and CFRP show substantially higher natural frequencies, implying improved vi- bration robustness within typical automotive excitation bands.

Mass-normalized stiffness-to-mass results

We assess stiffness-to-mass using displacement per mass proxy $\frac{\Delta}{\rho}$ (smaller is better for static stiffness/mass) and first-mode frequency per mass proxy $\frac{f_1}{\rho}$ (larger is better for dynamic stiffness/mass). With identical geometry, these are proportional to $\frac{\Delta}{m}$ and $\frac{f_1}{m}$. Values below use the representative design load LC2 (1,040 Pa).

Interpretation. Aluminum minimizes $\frac{\Delta}{\rho}$ (best static stiffness-per-mass); CFRP maximizes $\frac{f_1}{\rho}$ (best dynamic stiffness-per-mass); ABS trails on both.

Synthesis Considering static and dynamic responses together: aluminum provides high margins with minimal deformation; ABS is deformation-limited and fails at the highest load; CFRP achieves low displacement and adequate safety factors with governing compres- sion/shear limits. When normalized by mass, aluminum ranks best in static stiffness ($\frac{\Delta}{\rho}$) while CFRP ranks best in dynamic stiffness ($\frac{f_1}{\rho}$); see Table 9. These observations align with the governing-limit rationale outlined above

Table 3 Simulation results for Aluminum 6061-T6 under each aerodynamic load case.

Load Case	Max Tip Displacement (mm)	Peak Stress (MPa)	Safety Factor
LC-1 (520 Pa)	0.0537	14.088	22.00
LC-2 (1 040 Pa)	0.108	28.32	10.95
LC-3 (1 560 Pa)	0.162	42.48	7.30

Table 4 Simulation results for ABS under each aerodynamic load case.

Load Case	**Max Tip Displacement (mm)**	**Peak Stress (MPa)**	**Safety Factor**
LC-1 (520 Pa)	1.816	13.902	2.88
LC-2 (1,040 Pa)	3.630	27.803	1.44
LC-3 (1,560 Pa)	5.448	41.706	0.96

Table 5 Simulation results for Carbon Fiber under each aerodynamic load case.

Load Case	Max Tip Displacement (mm)	Peak Stress (MPa)	Safety Factor
LC-1 (520 Pa)	0.165	27.51	14.54
LC-2 (1 040 Pa)	0.330	55.02	7.27
LC-3 (1 560 Pa)	0.495	82.53	4.85

Table 6 Modal frequencies for ABS spoiler.

Mode	Frequency (Hz)
1	7.258
2	22.625
3	25.257
4	30.945
5	34.984
6	70.457

Table 7 Modal frequencies for Aluminum 6061-T6 spoiler.

Mode	Frequency (Hz)
1	25.738
2	80.297
3	89.722
4	109.660
5	124.000
6	250.500

Table 8 Modal frequencies for CFRP spoiler.

Mode	Frequency (Hz)
1	21.575
2	58.423
3	69.286
4	86.162
5	91.132
6	201.690

and support material selection toward aluminum or CFRP for the examined loading envelope.

Conclusion

This study quantified the structural response of a fixed-geometry rear spoiler across three materialsABS, aluminum 6061-T6, and quasi-isotropic CFRPsubjected to three representative aerodynamic pressures (520, 1 040, 1 560 Pa). Finite-element simulations reveal clear trade-offs:

Findings Aluminum delivered the smallest absolute deflections and the best static stiffness-to-mass (smallest $\frac{\Delta}{\rho}$), while CFRP offered the best dynamic stiffness-to-mass (largest $\frac{f_1}{\rho}$); ABS trailed on both mass-normalized metrics. ABS experienced large deflection (1.825.45 mm) and subcritical safety (SF 0.96 at 1 560 Pa), indicating probable failure; it is unsuitable for structurally loaded spoilers under high aerodynamic forces. A full failure mode assessmentincorporating the polymers nonlinear stressstrain response and a buck- ling eigenvalue studywould be required to predict post-yield behavior and local buckling of thin sections. Although beyond the current material-comparison scope, such analyses repre- sent important future work and do not affect the validity of comparing relative performance under identical loading. Modal analysis placed the first modes near 25.7 Hz (aluminum), 21.6 Hz (CFRP), and 7.26 Hz (ABS). Because the ABS first-mode frequency falls far short of the 30 Hz target, ABS is ruled out for this geometry unless major stiffening is introduced. These are below a typical 30 Hz target for components excited by road inputs, suggesting that modest structural stiffening and/or mounting refinements are warranted

© The National High School Journal of Science 2025

Table 9 Mass-normalized stiffness metrics at LC-2.

Material	ρ (g/cm^3)	Δ (mm)	Δ/ρ (mmcm^3/g)	f_1/ρ (Hzcm^3/g)
ABS	1.03	3.63	3.524	7.047
Al 6061-T6	2.70	0.108	0.0400	9.533
CFRP (quasi-iso)	1.60	0.330	0.206	13.484

to mitigate resonance risk[31].

Validation The structural deflection results obtained in this study were validated against published finite element analyses of automotive spoilers and wings under aerodynamic loading. Andreassi et al. conducted CFD-FEM coupled analysis of racing car wings under high- speed conditions, reporting wing tip deflections that produced 45% differences from rigid configurations when using carbon fiber materials with elastic moduli comparable to this study. Similarly, Geisbauer et al. performed structural analysis of Formula One rear wings and documented stress levels on the order of $6.36 \times 10^6 Pa$ under aerodynamic loading, which aligned with the stress magnitudes observed in our ABS and aluminum models. Our calculated tip deflections of 1.85.4 mm for the aluminum spoiler under 5201560 Pa loading compared favorably with NASA wing displacement studies, which demonstrated finite element prediction accuracies within 1.6% using similar computational methodologies. While direct experimental validation data for automotive spoiler deflection under the spe- cific loading conditions used in this study were limited in the open literature, the finite element methodology employed followed established protocols documented in aerospace and automo- tive structural analysis. The displacement-to-chord ratios and stress distribution patterns observed in our models fell within typical ranges reported for automotive exterior components under aerodynamic loading in motorsport applications. The primary contribution of this work lay in the systematic comparison of three distinct material systems under identical loading conditions rather than absolute deflection prediction, which maintained the validity of relative performance comparisons while acknowledging the limitations of absolute accuracy without direct experimental validation[32–36].

Limitations The loading was represented by uniform pressure fields derived from dynamic pressure; real distributions are nonuniform and depend on vehicle geometry, angle of attack, and local flow separation. The CFRP was modeled as a quasi-isotropic laminate without ply-level failure criteria; progressive damage or matrix/fiber failure were not evaluated. Fastener compliance and joint preload were approximated, and thermal/environmental effects were neglected. These choices are appropriate for a comparative material study but may over or underestimate local stress concentrations. Modal damping was not modeled; while this can substantially reduce resonant amplitudes, it produces only negligible shifts in natural frequencies at light damping, so the reported mode ordering and mass-normalized rankings are unaffected. Mount/body-panel compliance was not modeled; the pedestal bases were treated as fixed (rigid) supports. This idealization likely underestimates static deflections and overestimates natural frequencies, so the reported values should be interpreted as optimistic bounds with respect to boundary flexibility. Because geometry and loading are identical across materials, the effect is expected to act largely as a common-mode shift, and the qualitative material ranking reported here is expected to remain unchanged.

Future work (i) Couple fluidstructure interaction (FSI) to map realistic pressure fields and assess aeroelastic effects; (ii) incorporate laminate-level criteria for composites with pro- gressive damage; (iii) include detailed joint models (bolt preload, contact/friction) and vali- date against bench tests; and (iv) add mesh-refinement to remove any uncertainty. Overall, material selection exerts a first-order influence on spoiler structural performance: aluminum minimizes deflection for the studied geometry, CFRP provides superior performance per unit mass, and ABS should be avoided where significant aerodynamic loading is expected.

References

1 S. R. Cole, *Effects of spoiler surfaces on the aeroelastic behavior of a low-aspect- ratio rectangular wing*, Nasa langley research center technical report nasa tm-102622,.

2 R. V. Jr. Doggett, *Some effects of aerodynamic spoilers on wing flutter*, Nasa langley research center technical report nasa tm-101230,.

3 R. F. Gibson, *Principles of Composite Material Mechanics*, CRC Press, 4th edn.

4 *Composite materials handbook (cmh-17), volume 3: Polymer matrix composites ma- terials usage, design and analysis*, MIL-HDBK-17/3F (superseded by SAE R-424); Accessed 2025-08-08.

5 A. Karaki, M. A. Sirreya, M. Zalloum and H. Amro, *F1000Research*, **14**, year.

6 R. C. Das and M. Riyad, *Procedia engineering*, **194**, 160165.

7 S. Patel, S. Jogani, D. Chaklashiya, D. Chodvadiya, M. N. hara and V. Monpara, *International Research Journal of Engineering and Technology*, **11**, year.

8 W. Yu and L. Jiang, *International Journal of Automotive Manufacturing and Materials*, **3**, year.

9 T. T. ski and S. M. Najm., *Materials*, **17**, year.

10 M. Rejab, *Surface roughness optimization and machining research on 6061-t6 alu- minum, 2024. Google Scholar Profile - Research on aluminum 6061-T6 machining and automotive applications*.

11 I. S. Agustinus Purna Irawan, *International Journal of Mechanical Engineering and Technology (IJMET*, **1**, 915.

12 D. J. Naus, K. R. Corum and L. B. Klett, *Durability-based design criteria for a quasi-isotropic carbon-fiber-reinforced thermoplastic automotive composite*, Oak ridge national laboratory technical report ornl/tm-2006/011,.

13 Farnell, *Online PDF*.

14 Thomasnet, *Online Article*.

15 T. A. Composites, *Tc275-1 quasi-isotropic fabric technical paper*.

16 MatWeb, *Abs acrylonitrile butadiene styrene datasheet*, Ac- cessed September 24, 2025; Elastic modulus 2.2 GPa, shear modulus 0.8 GPa, Poissons.

17 J. Anderson, *EBOOK: Fundamentals of Aerodynamics (SI units)*, McGraw hill, 2011.

18 M. Cakir, *Mechanical Engineering Masters Theses*.

19 C.-H. Tsai, L.-M. Fu, C.-H. Tai, Y.-L. Huang and J.-C. Leong, *Applied Mathematical Modelling*, **33**, 36613673.

20 T. Schneider, Y. Hu, X. Gao, J. Dumas, D. Zorin and D. Panozzo, *ACM Transactions on Graphics (TOG*, **41**, 114.

21 M. P. Boyce, *Gas turbine engineering handbook*, Elsevier.

22 D. Syst'emes, *Viscous damping ratios for different systems and materials*.

23 Y. Dou, J. Zhang, X. Wen, H. Cheng and H. Liu, *Poly- mers*, **15**, year.

24 M. Department, *Natural frequency and damping ratio. Course Materials 18-03 Supplementary Notes 13*, Massachusetts Institute of Technology.

25 H. S. onnerlind., *COMSOL Blog*.

26 Z. Golubović, I. Danilov, B. Bojović, L. Petrov, A. Sedmak, Ž. Mišković and N. Mitrović, *Polymers*, 2023, **15**, 4197.

27 M. A. Dundar, G. S. Dhaliwal, E. Ayorinde and M. Al-Zubi, *Polymers and Polymer Composites*, **29**, 331342.

28 A. Li, J. Zhang, F. Zhang, L. Li, S. Zhu and Y. Yang, *New Carbon Materials*, **35**, 752761.

29 S. Nunna, A. R. Ravindran, J. Mroszczok, C. Creighton and R. J. Varley, *Composite Structures*, **303**, year.

30 K. Guseinov, O. Kudryavtsev, A. Bezmelnitsyn and S. Sapozhnikov, *Polymers*, **14**, year.

31 A. S. Y. Rashid, *The Scientific World Journal*.

32 S.-F. Lung and W. L. Ko, Congress of the International Council of the Aeronautical Sciences (ICAS 2016), 2016.

33 V. S. H. Kumar, *International Journal of Engineering and Advanced Technology (IJEAT*.

34 L. Andreassi, V. Mulone, P. P. Valentini and L. Vita, *A CFD-FEM Approach to Study Wing Aerodynamics under Deformation*, Sae technical paper technical report, 2004.

35 S. Patil, R. Lietz, S. Woodiga, H. Ahn, L. Larson, R. Gin, M. Elmore and A. Simpson, *Fluid Structure Interaction Simulations Applied to Automotive Aerodynamics*, Sae technical paper technical report, 2015.

36 D. Wood, M. A. Passmore and A.-K. Perry, *SAE International Journal of Passenger Cars-Mechanical Systems*, **7**, 145154.

 © The National High School Journal of Science 2025